INTERFACE FOCUS

royalsocietypublishing.org/journal/rsfs

Research

Cite this article: Clark GL, Pokutta-Paskaleva AP, Lawrence DJ, Lindsey SH, Desrosiers L, Knoepp LR, Bayer CL, Gleason Jr RL, Miller KS. 2019 Smooth muscle regional contribution to vaginal wall function. *Interface Focus* 20190025.
http://dx.doi.org/10.1098/rsfs.2019.0025

Accepted: 2 May 2019

One contribution of 13 to a theme issue 'Bioengineering for women's health, volume 1: female health and pathology'.

Subject Areas:
biomechanics, biomedical engineering, bioengineering

Keywords:
vagina, contractility, regional, smooth muscle, basal tone, biaxial

Author for correspondence:
Kristin S. Miller
e-mail: kmille11@tulane.edu

Electronic supplementary material is available online at rs.figshare.com.

THE ROYAL SOCIETY PUBLISHING

Smooth muscle regional contribution to vaginal wall function

Gabrielle L. Clark[1], Anastassia P. Pokutta-Paskaleva[2], Dylan J. Lawrence[1], Sarah H. Lindsey[3], Laurephile Desrosiers[4], Leise R. Knoepp[4], Carolyn L. Bayer[1], Rudolph L. Gleason Jr[5,2] and Kristin S. Miller[1]

[1]Department of Biomedical Engineering, Tulane University, 6823 St Charles Avenue, New Orleans, LA 70118, USA
[2]The Wallace H. Coulter Department of Biomedical Engineering, Georgia Institute of Technology, 801 Ferst Drive NW, Atlanta, GA 30332, USA
[3]Department of Pharmacology, Tulane University School of Medicine, 1430 Tulane Avenue, New Orleans, LA 70112, USA
[4]Department of Female Pelvic Medicine and Reconstructive Surgery, University of Queensland Ochsner Clinical School, 1514 Jefferson Highway, New Orleans, LA 70121, USA
[5]The George W. Woodruff School of Mechanical Engineering, Georgia Institute of Technology, Atlanta, GA, USA

CLB, 0000-0003-0947-6892; RLGJ, 0000-0002-6357-4955; KSM, 0000-0002-3462-6103

Pelvic organ prolapse is characterized as the descent of the pelvic organs into the vaginal canal. In the USA, there is a 12% lifetime risk for requiring surgical intervention. Although vaginal childbirth is a well-established risk factor for prolapse, the underlying mechanisms are not fully understood. Decreased smooth muscle organization, composition and maximum muscle tone are characteristics of prolapsed vaginal tissue. Maximum muscle tone of the vaginal wall was previously investigated in the circumferential or axial direction under uniaxial loading; however, the vaginal wall is subjected to multiaxial loads. Further, the contribution of vaginal smooth muscle basal (resting) tone to mechanical function remains undetermined. The objectives of this study were to determine the contribution of smooth muscle basal and maximum tone to the regional biaxial mechanical behaviour of the murine vagina. Vaginal tissue from C57BL/6 mice was subjected to extension–inflation protocols ($n = 10$) with and without basal smooth muscle tone. Maximum tone was induced with KCl under various circumferential ($n = 5$) and axial ($n = 5$) loading conditions. The microstructure was visualized with multiphoton microscopy ($n = 1$), multiaxial histology ($n = 4$) and multiaxial immunohistochemistry ($n = 4$). Smooth muscle basal tone decreased material stiffness and increased anisotropy. In addition, maximum vaginal tone was decreased with increasing intraluminal pressures. This study demonstrated that vaginal muscle tone contributed to the biaxial mechanical response of murine vaginal tissue. This may be important in further elucidating the underlying mechanisms of prolapse, in order to improve current preventative and treatment strategies.

1. Introduction

The female pelvic organs (uterus, bladder and rectum) are supported by pelvic floor muscles and fibromuscular tissues. Weakening of these structures may lead to the descent of the pelvic organs into the vaginal canal known as pelvic organ prolapse (POP). In the USA, there is a 12% lifetime risk for women to undergo pelvic reconstructive surgery restoring the anatomical position of the pelvic organs to alleviate symptoms (discomfort, defecatory dysfunction, incomplete bladder emptying, etc.) [1]. Clinical intervention for POP results in an annual expenditure over $1 billion [2]. Although vaginal childbirth, ageing and increased abdominal loading are well-established risk factors [3,4], the underlying mechanisms for POP are not fully understood.

The levator ani, a group of striated muscles, provides constant tone and structural support to the pelvic organs [5]. Injury during childbirth resulting in reduced muscle tone is a well-established mechanism for POP [6–8]; however, not all women with levator tears develop POP [7]. The vagina, a fibromuscular tissue, is suggested to play a role in providing pelvic organ support [5,9,10]. Vaginal smooth muscle (VaSM) organization [11,12], composition [11] and maximum muscle tone [13] are decreased in prolapsed tissues. Further, current surgical interventions using meshes to increase pelvic support negatively affect vaginal muscle tone [14].

Maximum and basal (resting) muscle tone are key characteristics of both striated and smooth muscle cells. The dominant clinical metric for assessing levator ani function is contractile strength or maximum muscle tone [15]. Basal tone, however, is negatively associated with POP indicating its importance [16]. Similarly, maximum tone of the vaginal wall is primarily investigated [13,14,17–21], but VaSM basal contribution may also be of significance [22–24]. Along the circumferential axis, maximum tone is greater in the proximal versus the distal region of the vaginal wall [18]. Regional variation may arise due to different embryological origins; the proximal vagina derives from the Müllerian ducts and the distal from the urogenital sinus [25,26].

Vaginal maximum tone was previously investigated by isometric contractile testing under a fixed extension on tissue strips taken along the circumferential [14,18] or axial direction [13,17,19,20]. The vaginal wall, however, is subjected to multiaxial loading within the body due to intra-abdominal pressures. Biaxial contractile testing permits application of multiaxial loads to better replicate physiological conditions [21,27]. Further, biaxial testing permits simultaneous quantification of muscle tone along the circumferential and axial axes [21]. Previously, planar biaxial testing was implemented to investigate smooth muscle maximum contribution to the mechanical behaviour of the rat vaginal wall [21]. In addition, extension–inflation protocols were leveraged to assess the contractile response of the porcine and murine arteries under isobaric-axially isometric contraction [27–29]. This methodology permits preservation of tissue geometry and smooth muscle-matrix interactions. Extension–inflation protocols have not been performed on murine vaginal tissue to assess muscle function. Rodent models are used to investigate biomechanical properties [30–34] and contractile function [17,18,20,21] of vaginal tissue. However, not a substitute for human tissue, similarities in the gross connective vaginal tissue anatomy are reported [32] and may provide insight into structure–function relationships.

Currently, it is not understood if VaSM dysfunction contributes to the pathogenesis of POP [35]. A lack in understanding may result from limited investigation of smooth muscle basal and maximum contribution to the biaxial mechanical response of vaginal tissue. Therefore, the objectives for this study are to (i) determine smooth muscle basal contribution to the biaxial mechanical behaviour of the proximal and distal vagina, and (ii) assess the regional contractile response under various circumferential and axial loads. We hypothesize that basal tone results in a decrease in outer diameter and material stiffness, further, that the proximal region is materially stiffer than the distal. As for maximum contraction, we hypothesize that higher loads (pressure and length) decrease the contractile response, and that the proximal region generates a greater contractile response than the distal.

2. Methods

Non-parous four to six months female C57BL6 J mice (24.4 ± 1.8 g; mean ± s.d.) (Jackson Laboratory, Bar Harbor, ME, USA, and Charles River, Wilmington, MA, USA) at oestrus were used throughout this study. Animals were housed under standard conditions (12 h light/dark cycles) and all procedures were approved by the Institute Animal Care and Use Committee at Tulane University. A pilot study (Jackson Lab ($n = 3$) and Charles River ($n = 3$)) revealed no significant differences in the mechanical properties of vaginal tissue between vendors. For functional and microstructural assessment, 29 animals were euthanized by guillotine without anaesthesia or carbon dioxide (CO_2) as outlined in figure 1. Upon sacrifice, the reproductive system was dissected immediately and placed in cold (4°C) Hank's Balanced Salt Solution, followed by separation of the vagina from the cervovaginal complex as illustrated previously by Robison *et al.* in figures 1 and 2 [33].

2.1. Biaxial mechanical testing

Extension–inflation testing was used to assess biaxial mechanical properties (figure 1*a*; $n = 10$), which permitted maintenance of native smooth muscle cell–matrix interactions and tissue geometry [33,34,36–38]. Freshly isolated vaginal tissue was mounted within a pressure-myograph system (Danish MyoTechnologies, Aarhus, Denmark) onto 3.75 mm diameter cannulas with two 6-0 sutures. The bath was filled with Krebs Ringer buffer (KRB; 120 mM NaCl, 25 mM $NaHCO_3$, 4.7 mM KCl, 2.5 mM $CaCl_2$, 1.2 mM NaH_2PO_4, 1.2 mM $MgCl_2$, 11 mM glucose) at 37°C aerated with 95% O_2 and 5% CO_2 to maintain pH at 7.4 for smooth muscle cell viability [27,39]. Custom acrylic housing prevented aeration interference with force measurements and outer diameter tracking [40]. The transducer-measured force and outer diameters were recorded via an integrated system of components (Eclipse TS100 video-microscope, Nikon, Melville, NY, USA) and software (Myoview Software, Danish MyoTechnologies, Aarhus, Denmark). The outer diameter for the proximal and distal regions was tracked 1.5 mm from the suture to minimize experimental variability due to end effects. This value was selected due to the proximal region ranging from 1.5 to 2.0 mm in length.

The unloaded configuration was defined as when the tissue was slightly buckled and not collapsed (3 mmHg) [33,34]. Post-explant, the vaginal tissue retracted in length [33,34,38]; therefore, in order to quantify tissue properties under near physiologically relevant loads, the tissue was axially extended [33,34,37,38,41] to an estimated physiologic length (1.15 times the unloaded length) [33,34]. Initial preconditioning was performed to minimize hysteresis with cyclic pressurization from 0 mmHg to the mean measured *in vivo* pressure (7 mmHg) over 5 cycles at 1.5 mmHg s^{-1} [33,42]. The mean measured *in vivo* pressure was determined by balloon catheterization as described and reported in electronic supplementary material figure S1). The physiologic length under basal tone was identified where the transducer-measured forces held constant over a range of increasing physiologic pressures [33,34,37,38,41]. Preconditioning with five cycles of pressurization (0–15 mmHg) at the physiologic length, and axial extension (10 µm s^{-1}) from 2% below to 2% above the physiologic length at a constant pressure (5 mmHg) was performed [33,34]. The tissue equilibrated for 10 min at the physiologic length under 5 mmHg, followed by re-establishment of the unloaded configuration [33].

The vaginal tissue was subjected to pressure–diameter testing (0–15 mmHg) over five cycles at and about (−2%, +2% and +4%) the physiologic length [33,34,37]. This was followed

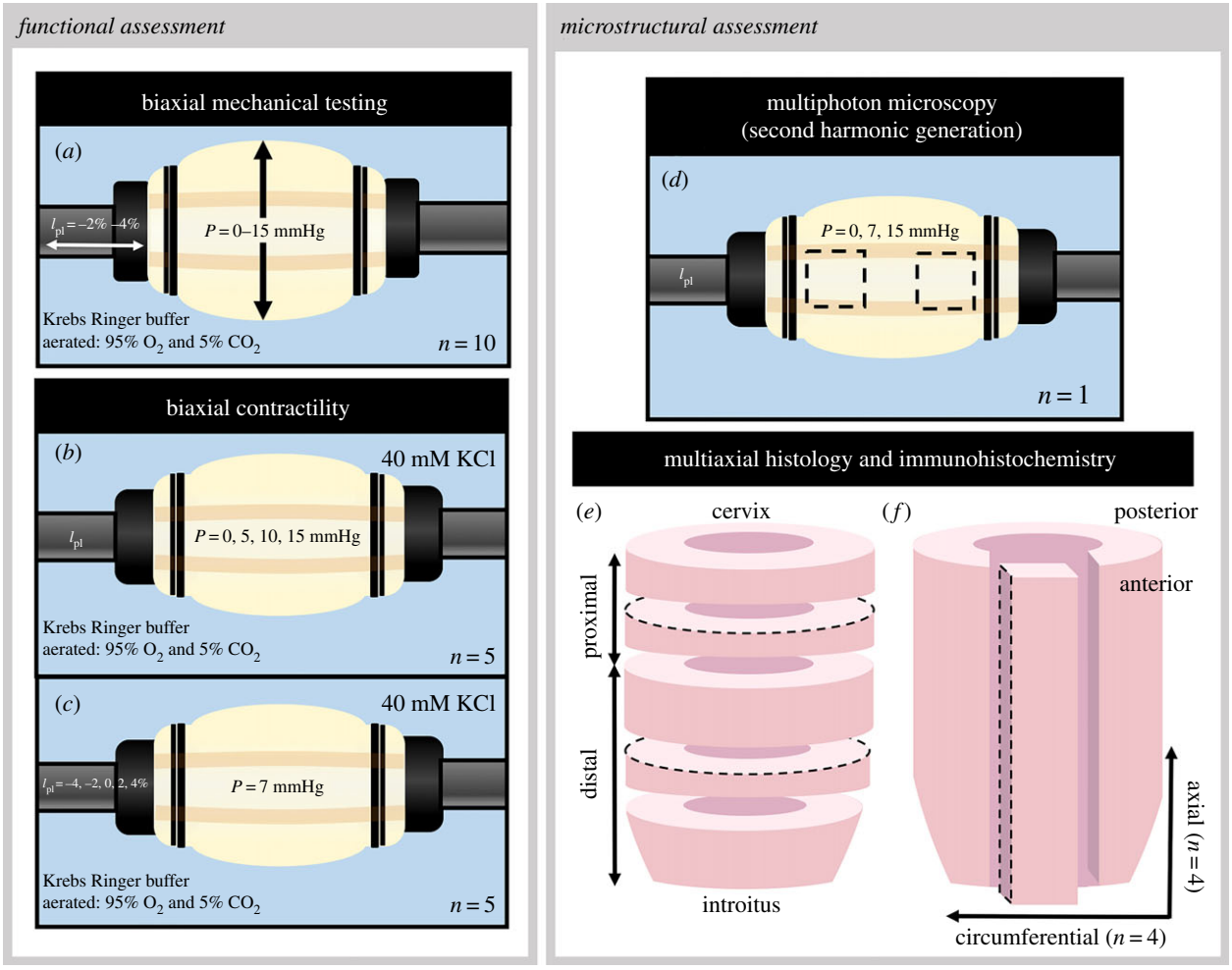

Figure 1. Schematic for functional and microstructural assessment of murine vaginal tissue. Tissues were subjected to extension–inflation protocols (*a*) for biaxial mechanical testing. Biaxial contractile testing was executed under various constant pressures (*b*) and fixed lengths (*c*). Multiphoton microscopy with SHG was performed at the averaged physiologic length along the anterior wall at the proximal and distal regions under three constant pressures (*d*). Histological and immunohistochemical analysis was performed on circumferential sections taken from the proximal and distal regions of the vaginal wall (*e*); axial sections were taken along the length of the anterior wall (*f*). The dashed lines represent the region of interest. (Online version in colour.)

by force–length testing to confirm the physiologic length [33,34,37,41]. The tissue was axially extended from 2% below to 2% above the physiologic length under four constant pressures: a tare load ($P = 2$ mmHg), 1/3 maximum pressure ($P = 5$ mmHg), 2/3 maximum pressure ($P = 10$ mmHg) and maximum pressure ($P = 15$ mmHg). Smooth muscle tone was removed by replacing the circulating medium with calcium-free KRB supplemented with 2 mM of a calcium-chelating agent, egtazic acid and incubated for 30 min [37,43]. Pressure–diameter tests were repeated at the relaxed (no tone) state under the same axial lengths as the basal state. Force–length tests were performed 2% above and below the physiologic length without smooth muscle tone.

2.2. Biaxial contractile testing

The evaluation of the biaxial contractile response with isobaric-axially isometric contraction under physiologically relevant loads (figure 1*b*,*c*) was performed with a pressure-myograph system [27,28,44]. Vaginal tissue was mounted and the unloaded configuration was determined, followed by initial preconditioning and identification of the physiologic length. For pressure-dependent contractility (figure 1*b*; $n = 5$), the tissue was preconditioned with five cycles of pressurization (0–15 mmHg), followed by re-establishing the unloaded configuration [33]. To maintain viability of the VaSM, preconditioning with maximum contraction was performed by stimulating the vaginal tissue under low loading conditions [27,28]. The intraluminal pressure was set to 5 mmHg and the vaginal tissue was axially stretched to a length from the unloaded length where the transducer-measured force equalled zero; followed by stimulation with 40 mM of potassium chloride (KCl) for 5 min until a steady response was achieved. This concentration induced maximal changes in force and outer diameter determined by a pilot study ($n = 5$). Following stimulation, the tissue was washed twice with KRB in order to return to basal tone. This was repeated at 9 mmHg, one standard deviation above the mean measured *in vivo* pressure [27,28]. The tissue was returned to its physiologic length for equilibration. After equilibration, the intraluminal pressure was set to 0 mmHg and contracted with 40 mM KCl then washed twice to return to basal tone. This was repeated to assess contraction as a function of intraluminal pressure at three constant pressures: 5, 10 and 15 mmHg.

To assess contraction as a function of axial length (figure 1*c*; $n = 5$), a separate cohort of animals was used due to the inability to restore basal outer diameter and force values after being contracted under higher circumferential and axial loads. It was imperative to obtain accurate stress values to determine the relationship between the stress and stretch response. Sample preparation and experimental set-up were conducted in the same manner; however, preconditioning was performed with five cycles of axial extension (10 $\mu m\ s^{-1}$) from 4% below to 4% above the physiologic length under a constant pressure (5 mmHg). Following smooth muscle preconditioning,

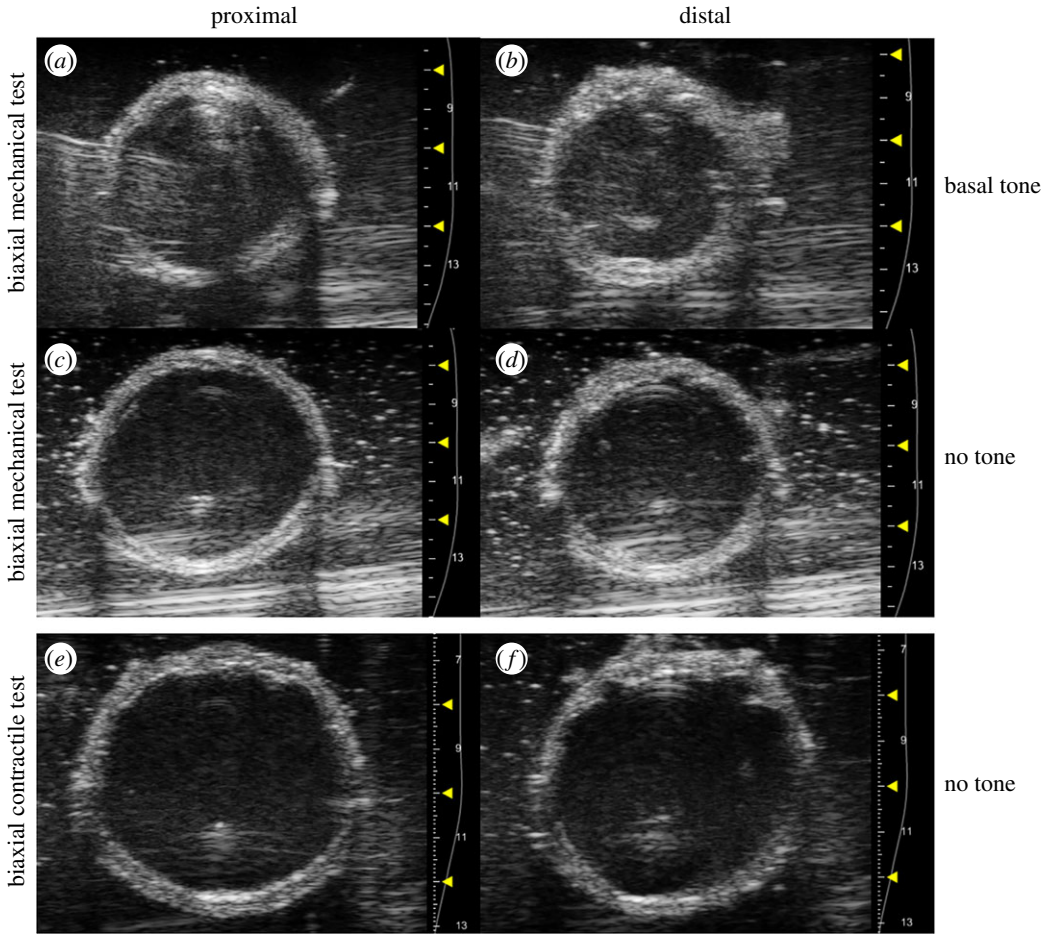

Figure 2. Representative ultrasound B-mode images acquired at the proximal (*a*,*c*,*e*) and distal (*b*,*d*,*f*) regions of the vaginal wall. During biaxial mechanical testing (*a*–*d*), images were acquired at the unloaded configuration with (*a*,*b*) and without (*c*,*d*) basal tone. For biaxial contractile testing (*e*,*f*), images were acquired at the unloaded configuration without muscle tone.

contraction as a function of axial length was assessed. Pressure was held constant at the mean measured *in vivo* pressure (7 mmHg), and the tissue was contracted at 4% and 2% below, above and at the physiologic length [27,33,34]. After contractile assessment, the passive state was induced and tissue geometry and force values were recorded [27,44].

2.3. Ultrasound imaging for vaginal wall thickness

Vaginal wall thickness was determined from ultrasound images acquired at the unloaded configuration for each state using the Vevo2100 ultrasound imaging system (FUJIFILM VisualSonics, Inc., Toronto, ON, Canada) [45]. Short-axis B-mode ultrasound images were obtained at each region of interest with a 40 MHz centre frequency transducer (LZ550) under basal tone and at the relaxed state for biaxial mechanical testing and the relaxed state for biaxial contractile testing (figure 2). The thickness of proximal and distal vagina were determined in ImageJ (NIH, Bethesda, MD, USA).

2.4. Mechanical testing and contractility data analysis

The unloaded volume was calculated at the proximal and distal region from the video-microscope unloaded outer radius, R_o, ultrasound unloaded thickness, H, and unloaded length, L, with basal tone and when relaxed. The unloaded regional length for the proximal and distal region was one-third and two-thirds of the total length, respectively, due to different embryological origins [25,26]. Assuming conservation of volume (i.e. incompressibility), the unloaded volume, regional deformed outer radius, r_o, and length, l, was used to calculate the deformed inner radius (r_i)

$$\bar{V} = \pi(R_o^2 - (R_o - H)^2)L \tag{2.1}$$

$$r_i = \sqrt{r_o^2 - \frac{\bar{V}}{\pi l}}. \tag{2.2}$$

The wall-averaged circumferential (θ), axial (z) and radial (r) Cauchy stresses (σ) were determined, where P is the intraluminal pressure and F_t is the transducer-measured force [37,46]

$$\sigma_\theta = \frac{Pr_i}{r_o - r_i}, \tag{2.3}$$

$$\sigma_z = \frac{F_t + \pi P r_i^2}{\pi(r_o^2 - r_i^2)}, \tag{2.4}$$

and

$$\sigma_r = \frac{Pr_i}{r_o + r_i}. \tag{2.5}$$

The change in stress with contraction ($\Delta\sigma$) was calculated by subtracting the passive stress where the VaSM was relaxed (σ^{relaxed}) from the total stress where the VaSM was maximally contracted ($\sigma^{\text{contracted}}$) [27,42,47,48]

$$\Delta\sigma_{\theta\theta} = \sigma_{\theta\theta}^{\text{contracted}} - \sigma_{\theta\theta}^{\text{relaxed}} + \sigma_{rr}^{\text{relaxed}} - \sigma_{rr}^{\text{contracted}} \tag{2.6}$$

and

$$\Delta\sigma_{zz} = \sigma_{zz}^{\text{contracted}} - \sigma_{zz}^{\text{relaxed}} + \sigma_{rr}^{\text{relaxed}} - \sigma_{rr}^{\text{contracted}}. \tag{2.7}$$

Circumferential stretch ratio (λ_θ) was defined by the radius at the mid-vaginal wall of the deformed state to the undeformed

state [37]. The axial stretch ratio (λ_z) was calculated as the axial length with respect to the relaxed unloaded axial length

$$\lambda_\theta = \frac{r_i + r_o/2}{R_i + R_o/2} \tag{2.8}$$

and

$$\lambda_z = \frac{l}{L}. \tag{2.9}$$

Compliance and tangent moduli were determined by taking the slope of the pressure–diameter and stress–strain curve within the physiologic pressure range (7 ± 2 mmHg; mean $\pm$ s.d.) at the physiologic length [49].

2.5. Multiphoton microscopy

Collagen fibre architecture of the anterior vaginal wall ($n = 1$) was visualized via second harmonic generation (SHG) at the average physiologic length (1.15 times the unloaded) under varied constant pressures (0, 7, 15 mmHg; figure 1*d*). As in experimental studies, a tare pressure of 3 mmHg was applied. The tissue was imaged with Zeiss 710 NLO inverted confocal microscope (Carl Zeiss Microscopy, LLC, Thornwood, NY, USA) in combination with a mode-locked Ti : Sapphire Chameleon Ultra laser (Coherent Inc., Santa Clara, CA, USA) equipped with non-descanned detector. Laser excitation was generated at 800 nm and backward SHG signal was collected in the 380–430 nm range with 40× oil immersion objective. Images were collected with the ZEN imaging software (Carl Zeiss Microscopy GmbH) at a resolution of 0.35×0.35 µm^2 per pixel at 8 bit pixel depth. Under each loading condition at the proximal and distal regions, three to four images were collected at a depth ranging between 7 and 10 µm from the adventitia. Collagen fibre angular distribution and alignment were quantified with an open source software, CurveAlign (LOCI, Madison, WI, USA; http://www.loci.wisc.edu/software/curvealign).

2.6. Multiaxial histology and immunohistochemistry

Specimens ($n = 8$) were fixed with 10% formalin for 24 h then paraffin embedded. Circumferential sections of 4 µm thickness ($n = 4$) were taken at the proximal and distal regions (figure 1*e*); axial sections of 4 µm thickness ($n = 4$) were taken along the anterior wall (figure 1*f*). For histological assessment, sections were stained with Masson's Trichrome and Hart's Elastin stain. Antigen retrieval for immunohistochemical analysis of α-smooth muscle actin (SMA) (Biocare, Pacheco, CA, USA) was performed for 15 min (pH = 6.0). Sections were blocked for 5 min in hydrogen peroxide and endogenous mouse IgG (Biocare, Pacheco, CA, USA) for 10 min. The sections were incubated for 30 min with the primary antibody (1 : 200) and detected with MACH 4 mouse probe (10 min) and rabbit polymer (10 min) (Biocare, Pacheco, CA, USA). Colour was developed by incubating in 3,3′ diaminobenzidine substrate for 5 min, followed by counterstaining with haematoxylin.

Brightfield images were taken using an Olympus BX51 microscope, an Olympus DP27 Digital Camera and cellSens™ software (Olympus Corporation, Center Valley, PA, USA) at 4× and 20× magnification. Area fraction quantification was performed on 4× images displaying the full cross-section with Colour Deconvolution, an open source plug-in for ImageJ, and a custom protocol using GNU Image Manipulation Program as previously described [34,50,51]. The epithelium, which is suggested to be non-load bearing, was excluded from this calculation [34,46].

2.7. Statistical analysis

To evaluate smooth muscle basal contribution to structural and material properties, paired *t*-tests were conducted on unloaded thickness, volume, physiologic length, physiologic outer diameter, compliance and tangent modulus comparing basal tone and no tone at each region. Differences in circumferential and axial tangent modulus were evaluated with paired *t*-tests. Regional differences were further evaluated with paired *t*-tests. For assessment of contractile response with loading, a one-way ANOVA with Tukey post hoc test was performed. The level for statistical significance was set at $p \leq 0.05$. A two-way ANOVA evaluated the effects of region and orientation on the change in stress with contraction and area fraction, followed by post hoc *t*-test and Bonferroni correction ($p < 0.05/2$) when necessary. All statistical analyses were performed in R (R Statistical Software, Vienna, Austria). The results are reported as mean $\pm$ standard error of the mean (s.e.m.). All experimental data were used in data analysis.

3. Results

3.1. Basal smooth muscle contribution to vaginal wall mechanical properties

Ultrasound imaging revealed a significant increase in unloaded thickness with basal tone compared to no tone for the proximal ($p < 0.05$) and distal ($p < 0.001$) regions (figure 3*a*). In addition, under basal tone unloaded thickness for the distal region was greater than the proximal ($p < 0.05$). Although unloaded volume with basal and no tone was greater at the distal region compared to the proximal ($p < 0.001$), significance was not identified between the two states at either regions (figure 3*b*). The physiologic outer diameter that was measured at the physiologic length and mean pressure (7 mmHg) displayed a significant decrease in the proximal region under basal tone ($p < 0.001$). Further, the physiologic outer diameter was significantly smaller for the distal region compared to the proximal with ($p < 0.05$) and without ($p < 0.001$) basal tone. The physiologic length was significantly shorter ($p < 0.001$) for the proximal and distal regions with the presence of basal tone (figure 3*d*). Basal tone induced a leftward shift in the pressure–diameter curve denoting a decrease in outer diameter compared to no tone (figure 4*a*). Basal tone induced a rightward shift in the stress–stretch curve denoting an increase in distensibility (figure 4*b*,*c*). Without basal tone, the distal region was more compliant ($p < 0.05$) than the proximal region (figure 4*d*). At the proximal region, basal tone resulted in a significant decrease ($p < 0.05$) in circumferential (figure 4*e*) and axial (figure 4*f*) tangent moduli. With basal tone, the circumferential tangent moduli was significantly larger than the axial for the proximal and distal regions ($p < 0.05$).

3.2. Vaginal contractile response to circumferential and axial loading

Stimulation with 40 mM KCl induced a tonic contraction resulting in a decrease in outer diameter and increase in axial force with reference to the relaxed state (figure 5*a*–*d*). The one-way ANOVA identified significant differences in the change in outer diameter with respect to intraluminal pressure for the proximal ($p < 0.05$) and distal ($p < 0.01$) regions (figure 5*a*). The change in diameter was reduced in proximal ($p < 0.05$) and distal ($p < 0.01$) regions between 0 and 15 mmHg. Further, the change in outer diameter with contraction was reduced ($p < 0.05$) at the distal region between 0 and 10 mmHg. The one-way ANOVA did not identify statistically significant differences in the change in

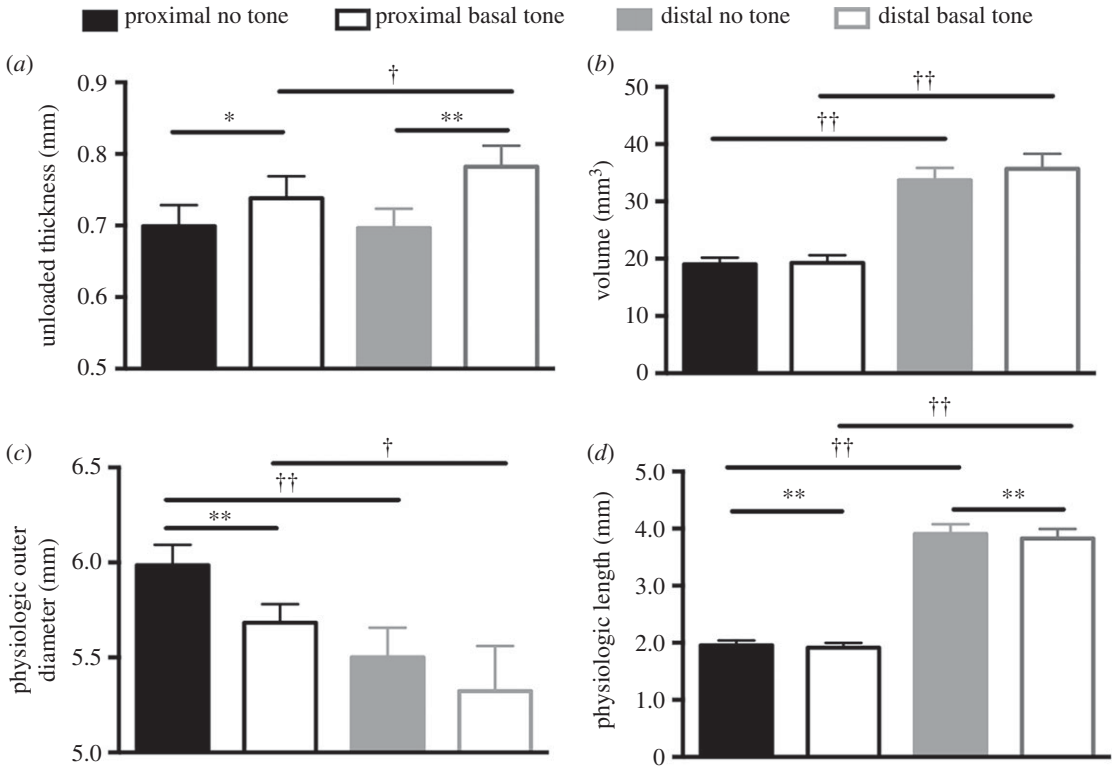

Figure 3. Basal tone resulted in a significant increase in the unloaded thickness at the proximal (black) and distal (grey) regions with the distal region being thicker than the proximal (*a*). The volume of the vagina was larger for the distal region compared to the proximal, with (open) and without (close) basal tone (*b*). Basal tone induced a significant decrease in outer diameter in the proximal region (*c*). The proximal region presented a larger outer diameter compared to distal, with and without basal tone. There was a decrease in physiologic length with basal tone for the proximal and distal regions (*d*). Data are reported as mean ± s.e.m. Statistical significance is denoted by state $^{*}p < 0.05$ and $^{**}p < 0.01$, as well as location $^{\dagger}p < 0.05$ and $^{\dagger\dagger}p < 0.01$.

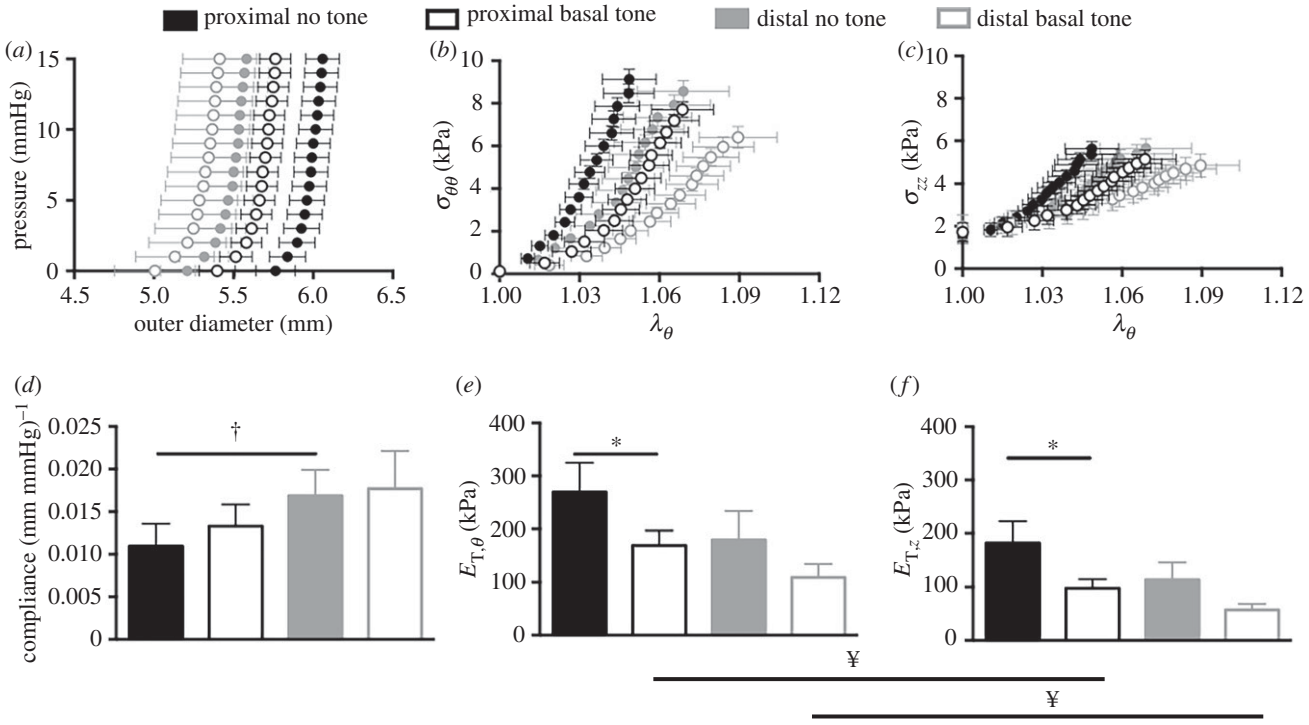

Figure 4. Vaginal wall outer diameter for the proximal (black) and distal (grey) regions as a function of increasing intraluminal pressure. Basal tone (open) resulted in a leftward shift in the pressure–diameter curve with respect to no tone (close) denoting decreased vaginal wall diameter (*a*). (*b*) Circumferential and (*c*) axial stresses at the physiologic length versus circumferential stretch. The presence of basal tone resulted in a rightward shift denoting an increase in distensibilty. The absence of basal tone resulted in a more complaint distal region compared to the proximal (*d*). (*e*) Basal tone decreased the circumferential and (*f*) axial tangent moduli at the proximal region. With basal tone, the circumferential tangent moduli was larger than the axial for both regions. Data are reported as mean ± s.e.m. Statistical significance ($p < 0.05$) is denoted by state *, location † and orientation ¥.

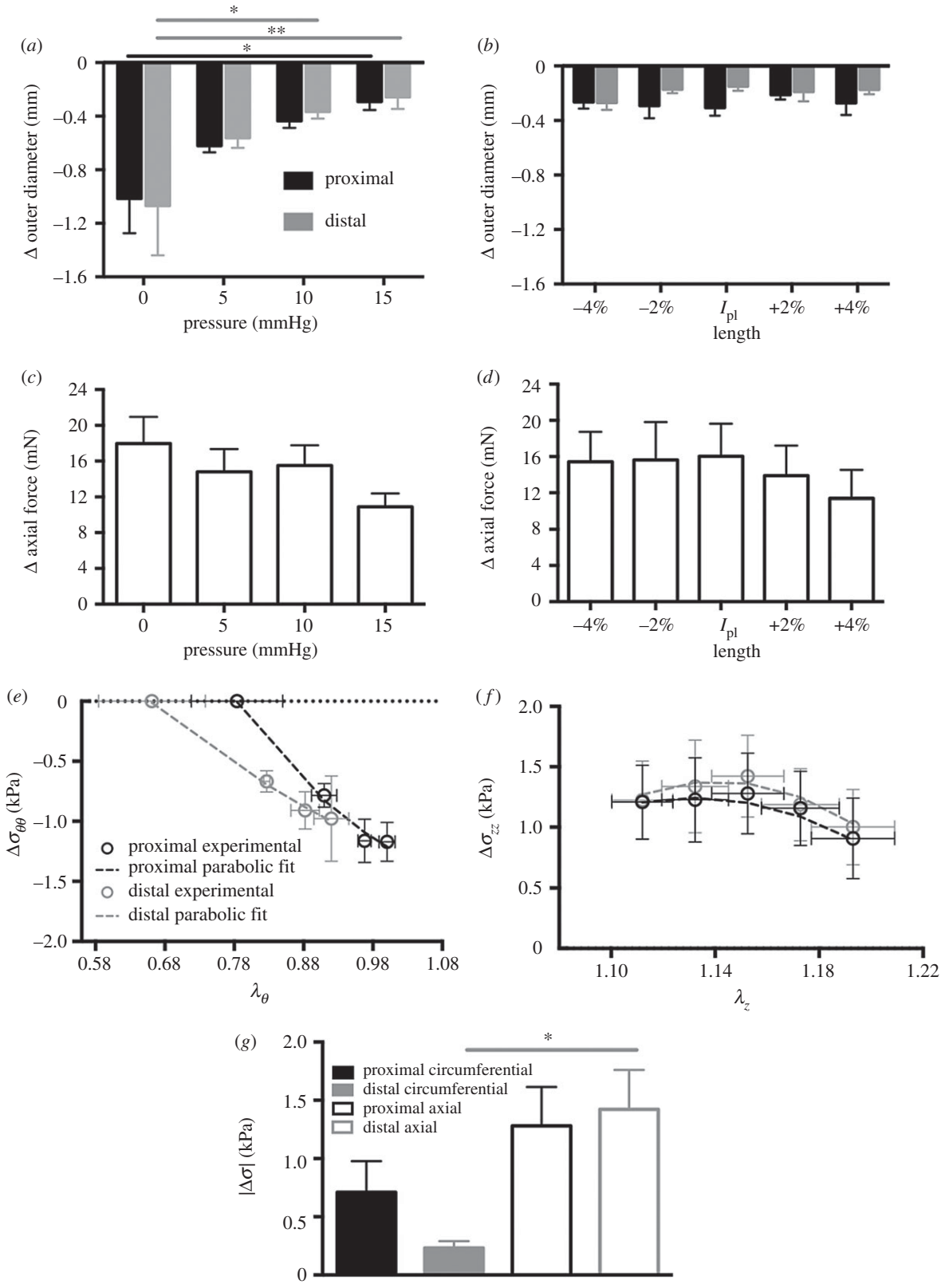

Figure 5. Change in outer diameter with contraction under various physiologically relevant pressures at the fixed physiologic length. The magnitude of the change in diameter with contraction was diminished at 15 mmHg for the proximal (black) and distal (grey) region, and 10 mmHg for the distal region only (*a*). Change in outer diameter with contraction at various physiologically relevant lengths under the mean measured *in vivo* pressure (*b*). Change in axial force with contraction under various physiologically relevant pressures at the fixed physiologic length (*c*). Change in axial force with contraction at various physiologically relevant lengths under the mean measured *in vivo* pressure (*d*). A parabolic function (dashed lines) described the changes in circumferential stress to circumferential stretch (RMSE; proximal = 0.09 and distal = 0.04) (*e*) and axial stress to axial stretch (RMSE; proximal = 0.09 and distal = 0.08) (*f*) curves. The absolute value of the change in stress at the physiologic length and pressure. At the distal region, axial stress was greater than circumferential stress (*g*). Data are reported as mean ± s.e.m. Statistical significance denoted by $*p < 0.05$ and $**p < 0.01$.

outer diameter as a function of change in axial length (figure 5*b*), nor the change in axial force as a function of pressure or axial length (figure 5*c*,*d*). Contraction resulted in a decrease in circumferential stress and increase in axial stress (figure 5*e*,*f*). A parabolic relationship ($\Delta\sigma = a(\lambda - h)^2 + k$) was observed for the change in circumferential

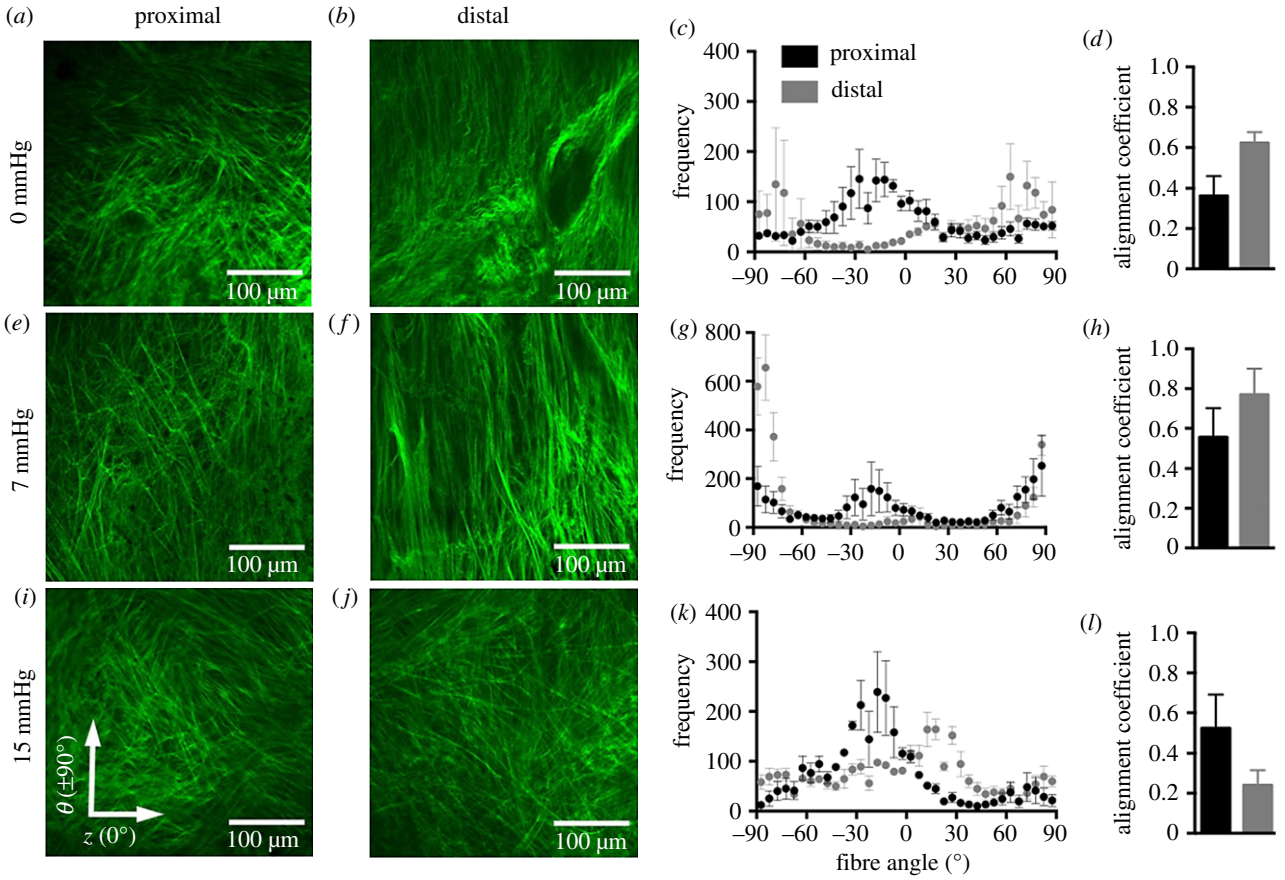

Figure 6. Multiphoton microscopy with SHG of collagen fibre architecture at the proximal (*a*,*e*,*i*) and distal (*b*,*f*,*j*) regions of the anterior vaginal wall under 0 (*a*,*b*), 7 (*e*,*f*) and 15 (*i*,*j*) mmHg at the average physiologic length. The frequency of the number of individual fibre segments with its respective orientation is reported with 0° denoting the axial axis and ±90° denoting the circumferential (*c*,*g*,*k*) at increments of 5°. At 0 and 7 mmHg, collagen fibres are oriented towards the circumferential axis at the distal region. At the proximal region, fibres are oriented towards the circumferential and diagonal axis (*c*,*g*). Under 15 mmHg, at the proximal and distal regions, the fibres are oriented towards the axial direction (*k*). The alignment coefficient describes collagen fibre orientation towards a preferred direction, with 1 being highly aligned (*d*,*h*,*l*). The alignment coefficient was larger for the distal region compared to the proximal at 0 and 7 mmHg. Data were averaged over several images and are reported as mean ± s.e.m. Imaging depth was 7–10 µm from the adventitial layer or outer wall. (Online version in colour.)

stress to circumferential stretch (RMSE; proximal = 0.09 and distal = 0.04; figure 5*e*) and axial stress to axial stretch (RMSE; proximal = 0.09 and distal = 0.08; figure 5*f*). The two-way ANOVA identified statistically significant differences ($p < 0.001$) with respect to orientation of the change in stress with contraction (figure 5*g*). At the distal region, the absolute value of axial stress was significantly higher ($p < 0.001$) than circumferential stress. As for the proximal region, a non-significant increase in axial stress ($p < 0.1$) was observed compared to circumferential.

3.3. Collagen fibre architecture under loading

Imaging of the collagen fibre architecture qualitatively and quantitatively demonstrated that at 0 and 7 mmHg, the proximal and distal regions exhibited marked differences in collagen fibre dispersion (figure 6*a*–*h*). At the distal region under 0 and 7 mmHg, collagen fibres displayed greater alignment towards the circumferential axis (±90°; figure 6*b*,*c*,*f*,*g*). The proximal region under 0 mmHg exhibited collagen fibres oriented towards the diagonal axis (30°; figure 6*a*,*c*); however, under 7 mmHg, fibres reoriented towards the circumferential axis (±90°; figure 6*e*,*g*). The proximal and distal regions were more aligned near the diagonal axis (±30°) towards the axial direction under 15 mmHg (figure 6*i*–*k*). The distal region presented a larger alignment coefficient, denoting that the distal region was more uniformly aligned towards a preferred direction compared to the proximal (figure 6*d*,*h*).

3.4. Regional multiaxial histological and immunohistochemical analysis

The two-way ANOVA identified statistically significant differences ($p < 0.01$) with respect to orientation in elastin area fraction. At the distal region, elastin area fraction was greater ($p < 0.01$) for axial sections (5.6 ± 0.6%) compared to circumferential (3.3 ± 0.6%) (figure 7*n*). The effect of region and orientation, however, were not found to be significant for collagen and α-SMA (figure 7*m*,*o*).

3.5. Contractility following elastase digestion

This study demonstrated that under maximum contraction, the distal region axial stress was greater than circumferential stress (figure 5*g*). Additionally, elastin area fraction was greater along the axial axis compared to circumferential (figure 7*n*). Prior work shows a decrease in elastin reduces the contractile response [27]. Therefore, a pilot study ($n = 5$) was conducted to investigate maximum contraction of the vaginal wall following elastase digestion. Experimental methods were performed as described in §2.4. Maximum contraction was performed at the physiologic length and mean pressure (7 mmHg), pre- and post-elastase digestion.

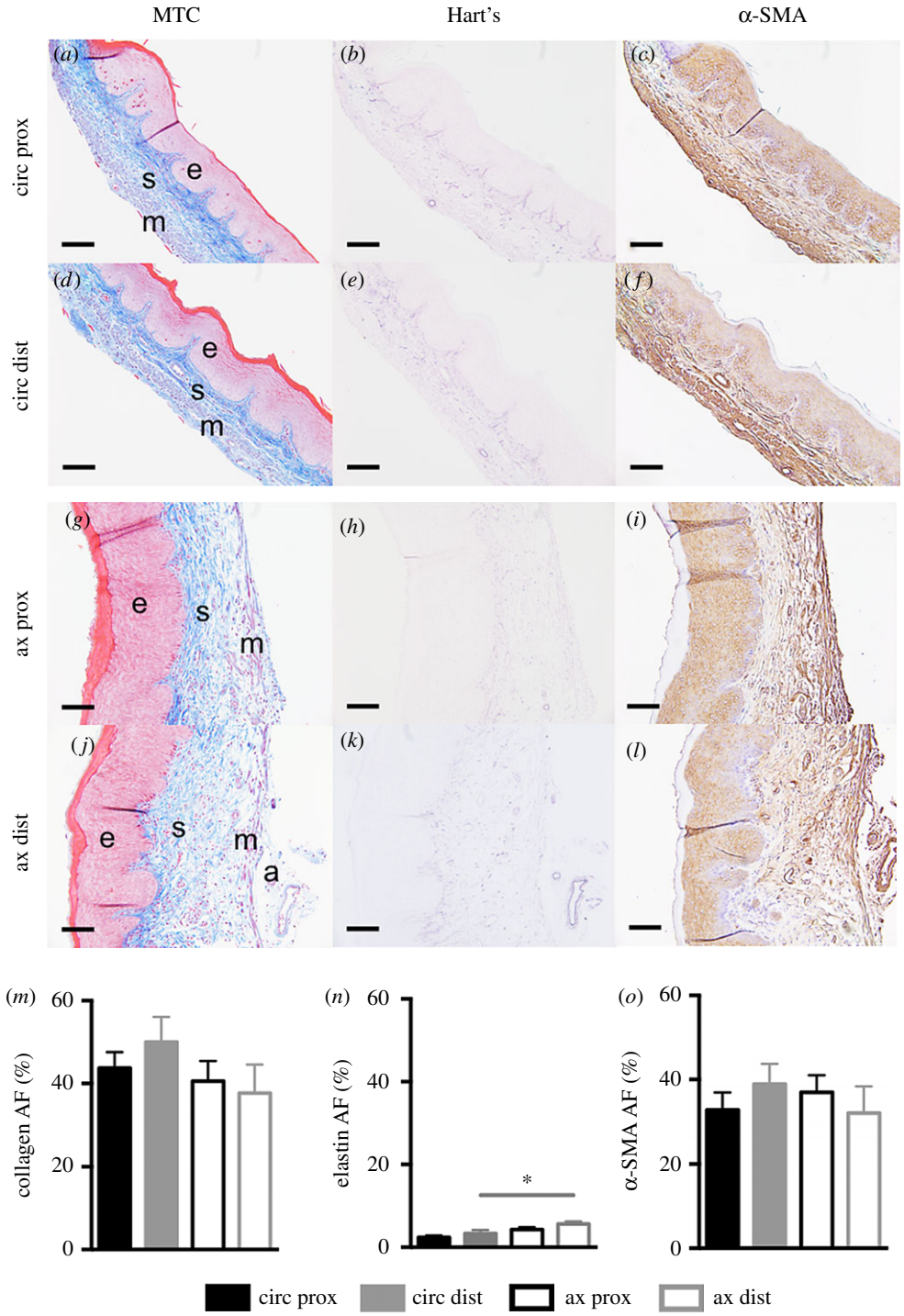

Figure 7. Representative histological images were acquired at 20× magnification. Proximal (prox; *a–c*, *g–i*) and distal (dist; *d–f*, *j–l*), circumferential (circ; *a–f*) and axial (ax; *g–l*) sections stained with Masson's Trichrome (MTC; *a*,*d*,*g*,*j*), Hart's Elastin (*b*,*e*,*h*,*k*) and α-SMA (*c*,*f*,*i*,*l*). Layers of the vaginal wall are denoted: epithelium (e), subepithelium (s), muscularis (m) and adventitia (a). Area fraction (AF) for collagen (M), elastin (N) and α-SMA (O) are reported for the proximal (black) and distal (grey) regions along the circumferential (close) and axial (open) sections. At the distal region, elastin area fraction was greater for the axial section compared to the circumferential. Data are reported as mean ± s.e.m. Statistical significance is denoted by $*p < 0.05/2$. Scale, 100 µm. (Online version in colour.)

The vaginal tissue was treated with 15 U of elastase for 45 min as described previously [34]. Elastase digestion significantly decreased ($p < 0.05$) the change in axial force with contraction (electronic supplementary material, figure S2B).

4. Discussion

This study presented the contribution of smooth muscle to the biaxial mechanical behaviour of the murine vaginal wall. The vaginal wall contains smooth muscle cells oriented primarily along the circumferential and axial axes. Further, the vaginal wall is subjected to multiaxial loading within the body. Therefore, within this study, extension–inflation protocols were used to assess basal smooth muscle tone contribution to the mechanical function of the vagina as well as to investigate maximum tone under various circumferential and axial loads. This permitted simultaneous characterization of smooth muscle contribution along the circumferential and axial axes. Smooth muscle basal and

maximum tone significantly contributed to the biaxial mechanical behaviour of the murine vaginal wall.

Smooth muscle basal tone significantly decreased vaginal length and outer diameter (figure 3*c*,*d*). These results coincide with changes in vaginal wall geometry induced by smooth muscle for sexual function [52,53]. An early physiological event of sexual arousal is characterized by pelvic nerve stimulation followed by smooth muscle relaxation. This induces an increase in vaginal length and diameter to permit penetration [52,53]. Further, basal tone significantly decreased material stiffness in the proximal region of the vagina (figure 4*e*,*f*). Material stiffness decreased with increased muscle tone (basal and maximum) in the rabbit basilar artery [23]. Kelly & Chowienczyk hypothesized that a decrease in muscle tone transfers loads to other components in the arterial wall, such as collagen fibres, increasing stiffness of the tissue [54]. This transfer of load may result in a decrease in collagen fibre undulation, thus increasing material stiffness. Therefore, we hypothesize that basal tone induces a transfer of load from collagen and elastic fibres to the smooth muscle cells increasing collagen fibre undulation thereby decreasing material stiffness of the vaginal wall.

Anisotropy, directional-dependent mechanical properties, of vaginal tissue was investigated by comparing the circumferential and axial tangent moduli. This study demonstrated that with basal tone, the circumferential direction was materially stiffer than the axial. Within this and a prior study, statistically significant differences in passive (no muscle tone) material stiffness between the circumferential and axial direction were not detected near the physiologically relevant configuration (length/axial stretch and pressure) [33]. In the previous study, anisotropy of the passive vagina was dependent on loading protocol [33]. This study, however, demonstrates that smooth muscle tone significantly contributes to the directional-dependent properties near physiologically relevant conditions. Investigation of anisotropy is useful for understanding disease progression. For example, the development of abdominal aortic aneurysms results in an increase in anisotropy, with a preference of material stiffening in the circumferential direction [55]. Understanding the vaginal wall, directional-dependent mechanical response may be useful for better understanding the development of POP.

In addition to smooth muscle basal contribution, maximum contribution was investigated as a function of mechanical loading. Maximum tone in the circumferential direction significantly decreased with increased intraluminal pressure (figure 5*a*). This response indicates that VaSM are sensitive to mechanical loading by pressure. This may be supported by prior observations that increased pressure results in arterial wall adaption mediated by smooth muscle cells in order to maintain a preferred homeostatic stress and restore material properties [22,56,57]. Perturbations to the mechanical environment and effect on vaginal function, however, are not defined. The vagina spends a majority of the time working within a mechanical environment under non-pregnant conditions. During pregnancy which is a brief period of time over a women's lifespan, the vaginal canal is subjected to extreme mechanical conditions that requires vaginal remodelling to permit passage of the foetus [17,58–60]. Although the vagina is able to withstand instantaneous changes in pressure outside of pregnancy [61], increased mechanical loading due to increased intra-abdominal pressure (i.e. chronic cough, constipation, repeated heavy lifting) is a risk factor for POP [62]. Therefore, the effect of sustained increased mechanical pressure on smooth muscle regulated mechano-mediated adaption merits further investigation in vaginal tissue.

For the murine vagina, a parabolic function described the regional stress–stretch curve behaviour under maximum contraction reasonably well (figure 5*e*,*f*). A parabolic relationship between active stress and stretch under isometric contraction is reasonable for vasculature [42,47,48] and the rat vaginal [21]. It was reported that the deformed state of the arterial wall alters the configuration of contractile proteins inside the smooth muscle cell dictating the active response [63]. Therefore, in addition to mechanical load, the change in stress with contraction depends on deformation (stretch).

The change in circumferential stress with contraction was not significantly different between the proximal and distal regions (figure 5*g*). This finding corresponds to rat vaginal tissue, wherein regional differences in maximum contraction along the circumferential axis were not detected in response to KCl [18]. The absolute value of the change in axial stress was significantly higher than circumferential stress at the distal region (figure 5*g*). This result is similar to the biaxial behaviour of the rat vagina. Stimulation with KCl induced a greater contractile response in the axial direction compared to the circumferential, by generating a higher active stress [21]. For the murine vagina, this result may be described by VaSM interaction with elastic fibres. At the distal region, elastin area fraction was greater on the axial axis compared to the circumferential axis (figure 7*n*). The pilot study ($n = 5$) demonstrated that removal of elastin significantly decreased axial force with contraction (electronic supplementary material, figure S2B). This corresponds to vasculature where the contractile response of the aorta from elastoplastic mice is decreased [27]. Therefore, the larger elastin area fraction along the axial axis of the murine vagina may result in a greater contractile response in the axial direction compared to the circumferential.

Additional microstructural analysis corresponded with mechanical findings. Regional differences in mechanical properties (figure 4) as well as collagen and elastic fibre area fraction were not identified (figure 7*m*,*n*). In addition to the composition of collagen and elastin [34,64–66], the organization of the fibres may dictate the mechanical response [67–69]. Although collagen fibres in the distal region were initially more highly aligned towards the circumferential axis (figure 6*a*–*h*), the tissue was not materially stiffer than the proximal region. This may result from imaging being performed between the adventitia and muscularis; however, collagen density is greater in the subepithelial layer (figure 7*a*,*d*,*g*,*j*). Additional analysis is needed throughout the thickness of the vaginal wall. Nevertheless, this study provides initial data on collagen fibre organization in the murine vagina, which is currently unknown. Lastly, regional differences in α-SMA were not detected. This corresponded to not observing regional differences in maximum contraction in response to KCL. Directional differences in maximum contraction were detected; however, differences in α-smooth actin were not identified. In addition to elastic fibres, other smooth muscle contractile proteins may be of significance [70,71].

This study is not without limitations. First, the vaginal wall was assumed to be incompressible. Although volume

change between the basal and passive state was not statistically significant, further investigation of isochoric motion is needed [27]. This study provides relevant data demonstrating smooth muscle contribution to the biaxial mechanical behaviour of murine vaginal tissue. Further, end effects (Saint-Venant's principle) were assumed to be negligible, although the aspect ratio of the murine vagina is nearly 1 : 1. Regardless, this study provides information on the regional behaviour where the proximal region is comparable to the distal. Experimental variability between the regions due to end effects were minimized by tracking the same distance away from the cannula. Alternatively, the cervovaginal complex could remain intact increasing the aspect ratio to minimize end effects. This, however, may induce additional artefacts to the force and diameter measurements due to murine cervical smooth muscle consisting of brief periods of both relaxation and contraction [39]. Therefore, coupling the cervix phasic behaviour to reduce end effects will lead to difficulty in independently evaluating vaginal wall basal and maximum tone.

5. Conclusion

Prior work focused on characterizing the passive uniaxial properties of vagina tissue [72–76]. Although this has provided initial valuable information to the field, it does not recapitulate the multiaxial loading the tissue experiences *in vivo*. Further, it does not account for the directional-dependent mechanical behaviour. In addition, the passive behaviour does not consider active smooth muscle interaction with the extracellular matrix and contribution to the mechanical properties. Recent work, however, highlights the significance of the biaxial properties and smooth muscle contribution to vaginal function [21,33,34]. This study investigated smooth muscle basal and maximum contribution to the proximal and distal region of the murine vaginal wall. Basal smooth muscle tone significantly contributed to the biaxial mechanical properties of the murine vagina. Further, the magnitude of circumferential contraction was significantly decreased with increased pressure and greater in the axial direction. The present findings suggest that vaginal active smooth muscle significantly interact with collagen and elastin contributing to the biaxial mechanical behaviour. Therefore, smooth muscle tone along the circumferential and axial axes should be evaluated when characterizing the mechanical properties of vaginal tissue. In addition to changes in collagen [77] and elastin [78] with prolapse, changes in smooth muscle composition and phenotype [11–13] may occur altering the mechanical behaviour of the tissue. Accounting for smooth muscle tone may aid in better understanding the functional changes that occurs with prolapse progression. Ultimately, this may assist in further elucidating the underlying mechanisms for prolapse, in order to improve current preventative and treatment strategies.

Data accessibility. Data available from the Dryad Digital Repository: https://doi.org/10.5061/dryad.98bb788.

Authors' contributions. G.L.C. carried out experimental design, mechanical and contractile test, data analysis and drafting of the manuscript; A.P.P.-P. carried out multiphoton imaging, data analysis and drafting of the manuscript; D.J.L. assisted in ultrasound imaging and drafting of the manuscript; K.S.M. participated in study design and drafting of the manuscript; all other authors (L.D., L.R.K., S.H.L., C.L.B., R.L.G.) contributed by scientific discussion and drafting of manuscript. All authors gave final approval for publication and agree to be held accountable for the work performed herein.

Competing interests. We declare we have no competing interests.

Funding. This work was funded by NSF Early Faculty CAREER Development Award CMMI-1751050 (K.S.M.); NSF CMMI-1727573 (R.L.G.); NIH HL133619 (S.H.L.); and the Louisiana Board of Regents Fellowship (G.L.C.).

Acknowledgements. We would like to acknowledge Sae-Il Murtada, PhD (Yale University), for training on biaxial contractile protocol. Further, we acknowledge Mary K. Clark and Monica Hanon (Georgia Institute of Technology) for assistance in multiphoton microscopy.

References

1. Wu JM, Matthews CA, Conover MM, Pate V, Funk MJ. 2014 Lifetime risk of stress urinary incontinence or pelvic organ prolapse surgery. *Obstet. Gynecol.* **123**, 1201–1206. (doi:10.1097/AOG.0000000000000286)
2. Subak LL, Waetjen LE, van den Eeden S, Thom DH, Vittinghoff E, Brown JS. 2001 Cost of pelvic organ prolapse surgery in the United States. *Obstet. Gynecol.* **98**, 646–651. (doi:10.1097/00006250-200110000-00021)
3. Mant J, Painter R, Vessey M. 1997 Epidemiology of genital prolapse: observations from the Oxford Family Planning Association Study. *Br. J. Obstet. Gynaecol.* **104**, 579–585. (doi:10.1111/j.1471-0528.1997.tb11536.x)
4. Hendrix SL, Clark A, Nygaard I, Aragaki A, Barnabei V, McTiernan A. 2002 Pelvic organ prolapse in the Women's Health Initiative: gravity and gravidity. *Am. J. Obstet. Gynecol.* **186**, 1160–1166. (doi:10.1067/mob.2002.123819)
5. Delancey JOL. 1992 Anatomic aspects of vaginal eversion after hysterectomy. *Am. J. Obstet. Gynecol.* **166**, 1717–1728. (doi:10.1016/0002-9378(92)91562-0)
6. Benson T, Weidner AC. 2000 Pelvic muscle electromyography of levator ani and external anal sphincter in nulliparous women and women with pelvic floor dysfunction—discussion. *Am. J. Obstet. Gynecol.* **183**, 1390–1401. (doi:10.1067/mob.2000.111073)
7. DeLancey JOL *et al.* 2007 Comparison of levator ani muscle defects and function in women with and without pelvic organ prolapse. *Obstet. Gynecol.* **109**, 295–302. (doi:10.1097/01.AOG.0000250901.57095.ba)
8. Friedman S, Blomquist JL, Nugent JM, McDermott KC, Munoz A, Handa VL. 2012 Pelvic muscle strength after childbirth. *Obstet. Gynecol.* **120**, 1021–1028. (doi:10.1097/aog.0b013e318265de39)
9. Liu XQ, Zhao Y, Pawlyk B, Damaser M, Li TS. 2006 Failure of elastic fiber homeostasis leads to pelvic floor disorders. *Am. J. Pathol.* **168**, 519–528. (doi:10.2353/ajpath.2006.050399)
10. Wieslander CK, Rahn DD, McIntire DD, Acevedo JF, Drewes PG, Yanagisawa H, Word RA. 2009 Quantification of pelvic organ prolapse in mice: vaginal protease activity precedes increased MOPQ scores in Fibulin 5 knockout mice. *Biol. Reprod.* **80**, 407–414. (doi:10.1095/biolreprod.108.072900)
11. Boreham MK, Wai CY, Miller RT, Schaffer JI, Word RA. 2002 Morphometric analysis of smooth muscle in the anterior vaginal wall of women with pelvic organ prolapse. *Am. J. Obstet. Gynecol.* **187**, 56–63. (doi:10.1067/mob.2002.124843)
12. Badiou W, Granier G, Bousquet PJ, Monrozies X, Mares P, de Tayrac R. 2008 Comparative histological analysis of anterior vaginal wall in women with pelvic organ prolapse or control subjects. A pilot study. *Int. Urogynecol. J.* **19**, 723–729. (doi:10.1007/s00192-007-0516-4)
13. Northington GM, Basha M, Arya LA, Wein AJ, Chacko S. 2011 Contractile response of human anterior vaginal muscularis in women with and without pelvic organ prolapse. *Reprod. Sci.* **18**, 296–303. (doi:10.1177/1933719110392054)
14. Jallah Z, Liang R, Feola A, Barone W, Palcsey S, Abramowitch SD, Yoshimura N, Moalli P. 2016 The

impact of prolapse mesh on vaginal smooth muscle structure and function. *Bjog Int. J. Obstet. Gynaecol.* **123**, 1076–1085. (doi:10.1111/1471-0528.13514)

15. Theofrastous JP, Swift SE. 1998 The clinical evaluation of pelvic floor dysfunction. *Obstet. Gynecol. Clin. North Am.* **25**, 783–804. (doi:10.1016/S0889-8545(05)70043-7)
16. Dietz HP, Shek KL. 2008 The quantification of levator muscle resting tone by digital assessment. *Int. Urogynecol. J.* **19**, 1489–1493. (doi:10.1007/s00192-008-0682-z)
17. Feola A, Moalli P, Alperin M, Duerr R, Gandley RE, Abramowitch S. 2011 Impact of pregnancy and vaginal delivery on the passive and active mechanics of the rat vagina. *Ann. Biomed. Eng.* **39**, 549–558. (doi:10.1007/s10439-010-0153-9)
18. Skoczylas LC, Jallah Z, Sugino Y, Stein SE, Feola A, Yoshimura N, Moalli P. 2013 Regional differences in rat vaginal smooth muscle contractility and morphology. *Reprod. Sci.* **20**, 382–390. (doi:10.1177/1933719112472733)
19. Basha M, Chang SH, Smolock EM, Moreland RS, Wein AJ, Chacko S. 2006 Regional differences in myosin heavy chain isoform expression and maximal shortening velocity of the rat vaginal wall smooth muscle. *Am. J. Physiol. -Regul. Integr. Comp. Physiol.* **291**, R1076–R1084. (doi:10.1152/ajpregu.00118.2006)
20. Basha M, LaBelle EF, Northington GM, Wang TC, Wein AJ, Chacko S. 2009 Functional significance of muscarinic receptor expression within the proximal and distal rat vagina. *Am. J. Physiol. Regul. Integr. Comp. Physiol.* **297**, R1486–R1493. (doi:10.1152/ajpregu.90516.2008)
21. Huntington A, Rizzuto E, Abramowitch S, Del Prete Z, De Vita R. 2018 Anisotropy of the passive and active rat vagina under biaxial loading. *Ann. Biomed. Eng.* **47**, 272–281. (doi:10.1007/s10439-018-02117-9)
22. Fridez P, Makino A, Miyazaki H, Meister JJ, Hayashi K, Stergiopulos N. 2001 Short-term biomechanical adaptation of the rat carotid to acute hypertension: contribution of smooth muscle. *Ann. Biomed. Eng.* **29**, 26–34. (doi:10.1114/1.1342054)
23. Baek S, Gleason RL, Rajagopal KR, Humphrey JD. 2007 Theory of small on large: potential utility in computations of fluid–solid interactions in arteries. *Comput. Methods Appl. Mech. Eng.* **196**, 3070–3078. (doi:10.1016/j.cma.2006.06.018)
24. Jankowski RJ, Prantil RL, Fraser MO, Chancellor MB, de Groat WC, Huard J, Vorp DA. 2004 Development of an experimental system for the study of urethral biomechanical function. *Am. J. Physiol. -Renal Physiol.* **286**, F225–FF32. (doi:10.1152/ajprenal.00126.2003)
25. Makiyan Z. 2016 New theory of uterovaginal embryogenesis. *Organogenesis* **12**, 33–41. (doi:10.1080/15476278.2016.1145317)
26. Mazloomdoost D, Westermann LB, Mutema G, Crisp CC, Kleeman SD, Pauls RN. 2017 Histologic anatomy of the anterior vagina and urethra. *Female Pelvic Med. Reconstr. Surg.* **23**, 329–335. (doi:10.1097/SPV.0000000000000387)
27. Murtada SI, Ferruzzi J, Yanagisawa H, Humphrey JD. 2016 Reduced biaxial contractility in the descending thoracic aorta of fibulin-5 deficient mice. *J. Biomech. Eng. -Trans. Asme* **138**, 051008. (doi:10.1115/1.4032938)
28. Ferruzzi J, Murtada SI, Li GX, Jiao Y, Uman S, Ting MYL, Tellides G, Humphrey JD. 2016 Pharmacologically improved contractility protects against aortic dissection in mice with disrupted transforming growth factor-beta signaling despite compromised extracellular matrix properties. *Arterioscl. Thromb. Vasc. Biol.* **36**, 919–927. (doi:10.1161/ATVBAHA.116.307436)
29. Tanko LB, Mikkelsen EO, Frobert O, Bagger JP, Gregersen H. 1998 A new method for combined isometric and isobaric pharmacodynamic studies on porcine coronary arteries. *Clin. Exp. Pharmacol. Physiol.* **25**, 919–927. (doi:10.1111/j.1440-1681.1998.tb02344.x)
30. Lowder JL, Debes KM, Moon DK, Howden N, Abramowitch SD, Moalli PA. 2007 Biomechanical adaptations of the rat vagina and supportive tissues in pregnancy to accommodate delivery. *Obstet. Gynecol.* **109**, 136–143. (doi:10.1097/01.AOG.0000250472.96672.6c)
31. Moalli PA, Debes KM, Meyn LA, Howden NS, Abramowitch SD. 2008 Hormones restore biomechanical properties of the vagina and supportive tissues after surgical menopause in young rats. *Am. J. Obstet. Gynecol.* **199**, 161.e1–161.e8. (doi:10.1016/j.ajog.2008.01.042)
32. Moalli PA, Howden NS, Lowder JL, Navarro JM, Debes KM, Abramowitch SD, Woo SL. 2005 A rat model to study the structural properties of the vagina and its supportive tissues. *Am. J. Obstet. Gynecol.* **192**, 80–88. (doi:10.1016/j.ajog.2004.07.008)
33. Robison KM, Conway CK, Desrosiers L, Knoepp LR, Miller KS. 2017 Biaxial mechanical assessment of the murine vaginal wall using extension-inflation testing. *J. Biomech. Eng. -Trans. Asme* **139**, 104504. (doi:10.1115/1.4037559)
34. Akintunde A, Robison KM, Capone D, Desrosiers L, Knoepp LR, Miller KS. 2018 Effects of elastase digestion on the murine vaginal wall biaxial mechanical response. *J. Biomech. Eng.* **14**, 021011. (doi:10.1115/1.4042014)
35. Mei SS, Ye M, Gil L, Zhang JP, Zhang YP, Candiotti K, Takacs P. 2013 The role of smooth muscle cells in the pathophysiology of pelvic organ prolapse. *Female Pelvic Med. Reconstr. Surg.* **19**, 254–259. (doi:10.1097/SPV.0b013e31829ff74d)
36. Gleason RL, Gray SP, Wilson E, Humphrey JD. 2004 A multiaxial computer-controlled organ culture and biomechanical device for mouse carotid arteries. *J. Biomech. Eng. -Trans. Asme* **126**, 787–795. (doi:10.1115/1.1824130)
37. Ferruzzi J, Bersi MR, Humphrey JD. 2013 Biomechanical phenotyping of central arteries in health and disease: advantages of and methods for murine models. *Ann. Biomed. Eng.* **41**, 1311–1330. (doi:10.1007/s10439-013-0799-1)
38. Amin M, Le VP, Wagenseil JE. 2012 Mechanical testing of mouse carotid arteries: from newborn to adult. *Jove-J. Vis. Exp.* **60** pii: 3733. (doi:10.3791/3733)
39. Gravina FS, van Helden DF, Kerr KP, de Oliveira RB, Jobling P. 2014 Phasic contractions of the mouse vagina and cervix at different phases of the estrus cycle and during late pregnancy. *PLoS ONE* **9**, e111307. (doi:10.1371/journal.pone.0111307)
40. Baah-Dwomoh A, De Vita R. 2017 Effects of repeated biaxial loads on the creep properties of cardinal ligaments. *J. Mech. Behav. Biomed. Mater.* **74**, 128–141. (doi:10.1016/j.jmbbm.2017.05.038)
41. Vanloon P, Klip W, Bradley E. 1977 Length-force and volume–pressure relationships of arteries. *Biorheology* **14**, 181–201. (doi:10.3233/BIR-1977-14405)
42. Zhou B, Rachev A, Shazly T. 2015 The biaxial active mechanical properties of the porcine primary renal artery. *J. Mech. Behav. Biomed. Mater.* **48**, 28–37. (doi:10.1016/j.jmbbm.2015.04.004)
43. Ashoori F, Takai A, Tomita T. 1985 The response of non-pregnant rat myometrium to oxytocin in Ca-free solution. *Br. J. Pharmacol.* **84**, 175–183.
44. Caulk AW, Nepiyushchikh ZV, Shaw R, Dixon JB, Gleason RL. 2015 Quantification of the passive and active biaxial mechanical behaviour and microstructural organization of rat thoracic ducts. *J. R. Soc. Interface* **12**, 20150280. (doi:10.1098/rsif.2015.0280)
45. Panayi DC, Digesu GA, Tekkis P, Fernando R, Khullar V. 2010 Ultrasound measurement of vaginal wall thickness: a novel and reliable technique. *Int. Urogynecol. J.* **21**, 1265–1270. (doi:10.1007/s00192-010-1183-4)
46. Humphrey JD. 2002 *Cardiovascular solid mechanics: cells, tissues, and organs*. Berlin, Germany: Springer.
47. Agianniotis A, Rachev A, Stergiopulos N. 2012 Active axial stress in mouse aorta. *J. Biomech.* **45**, 1924–1927. (doi:10.1016/j.jbiomech.2012.05.025)
48. Zhou B, Prim DA, Romito EJ, McNamara LP, Spinale FG, Shazly T, Eberth JF. 2018 Contractile smooth muscle and active stress generation in porcine common carotids. *J. Biomech. Eng. -Trans. Asme* **140**, 014501. (doi:10.1115/1.4037949)
49. Stoka KV, Maedeker JA, Bennett L, Bhayani SA, Gardner WS, Procknow JD, Cocciolone AJ, Walji TA, Craft CS, Wagenseil JE. 2018 Effects of increased arterial stiffness on atherosclerotic plaque amounts. *J. Biomech. Eng. -Trans. Asme* **140**, 051007. (doi:10.1115/1.4039175)
50. Ruifrok AC, Johnston DA. 2001 Quantification of histochemical staining by color deconvolution. *Anal. Quant. Cytol. Histol.* **23**, 291–299.
51. Capone DJ, Clark GL, Bivona D, Ogola BO, Desrosiers L, Knoepp LR, Lindsey SH, Miller KS. Evaluating residual strain throughout the murine female reproductive system. *J. Biomech.* **82**, 299–306. (doi:10.1016/j.jbiomech.2018.11.001)
52. Park K, Goldstein I, Andry C, Siroky MB, Krane RJ, Azadzoi KM. 1997 Vasculogenic female sexual dysfunction: the hemodynamic basis for vaginal engorgement insufficiency and clitoral erectile

insufficiency. *Int. J. Impot. Res.* **9**, 27–37. (doi:10.1038/sj.ijir.3900258)

53. Berman JR. 2005 Physiology of female sexual function and dysfunction. *Int. J. Impot. Res.* **17**, S44–S51. (doi:10.1038/sj.ijir.3901428)
54. Kelly BA, Chowienczyk P. 2002 An introduction to vascular biology. In *An introduction to vascular biology* (ed. BJ Hunt), pp. 33–48. Cambridge, UK: Cambridge University Press.
55. Geest JPV, Sacks MS, Vorp DA. 2006 The effects of aneurysm on the biaxial mechanical behavior of human abdominal aorta. *J. Biomech.* **39**, 1324–1334. (doi:10.1016/j.jbiomech.2005.03.003)
56. Fridez P, Makino A, Kakoi D, Miyazaki H, Meister JJ, Hayashi K, Stergiopulos N. 2002 Adaptation of conduit artery vascular smooth muscle tone to induced hypertension. *Ann. Biomed. Eng.* **30**, 905–916. (doi:10.1114/1.1507326)
57. Humphrey JD, Dufresne ER, Schwartz MA. 2014 Mechanotransduction and extracellular matrix homeostasis. *Nat. Rev. Mol. Cell Biol.* **15**, 802–812. (doi:10.1038/nrm3896)
58. Daucher JA, Clark KA, Stolz DB, Meyn LA, Moalli PA. 2007 Adaptations of the rat vagina in pregnancy to accommodate delivery. *Obstet. Gynecol.* **109**, 128–135. (doi:10.1097/01.AOG.0000246798.78839.62)
59. Wieslander CK, Marinis SI, Drewes PG, Keller PW, Acevedo JF, Word RA. 2008 Regulation of elastolytic proteases in the mouse vagina during pregnancy, parturition, and puerperium. *Biol. Reprod.* **78**, 521–528. (doi:10.1095/biolreprod.107.063024)
60. Ulrich D, Edwards SL, Su K, White JF, Ramshaw JAM, Jenkin G, Deprest J, Rosamilia A, Werkmeister JA, Gargett CE. 2014 Influence of reproductive status on tissue composition and biomechanical properties of ovine vagina. *PLoS ONE* **9**, e93172. (doi:10.1371/journal.pone.0093172)
61. Kruger J, Hayward L, Nielsen P, Loiselle D, Kirton R. 2013 Design and development of a novel intra-vaginal pressure sensor. *Int. Urogynecol. J.* **24**, 1715–1721. (doi:10.1007/s00192-013-2097-8)
62. Miedel A, Tegerstedt G, Maehle-Schmidt M, Nyren O, Hammarstrom M. 2009 Nonobstetric risk factors for symptomatic pelvic organ prolapse. *Obstet. Gynecol.* **113**, 1089–1097. (doi:10.1097/AOG.0b013e3181a11a85)
63. Rachev A, Hayashi K. 1999 Theoretical study of the effects of vascular smooth muscle contraction on strain and stress distributions in arteries. *Ann. Biomed. Eng.* **27**, 459–468. (doi:10.1114/1.191)
64. Fan YH, Zhao JB, Liao DH, Gregersen H. 2005 The effect of digestion of collagen and elastin on histomorphometry and the zero-stress state in rat esophagus. *Dig. Dis. Sci.* **50**, 1497–1505. (doi:10.1007/s10620-005-2868-2)
65. Gundiah N, Babu AR, Pruitt LA. 2013 Effects of elastase and collagenase on the nonlinearity and anisotropy of porcine aorta. *Physiol. Meas.* **34**, 1657–1673. (doi:10.1088/0967-3334/34/12/1657)
66. Pichamuthu JE, Phillippi JA, Cleary DA, Chew DW, Hempel J, Vorp DA, Gleason TG. 2013 Differential tensile strength and collagen composition in ascending aortic aneurysms by aortic valve phenotype. *Ann. Thorac. Surg.* **96**, 2147–2154. (doi:10.1016/j.athoracsur.2013.07.001)
67. Chen H, Liu Y, Slipchenko MN, Zhao XF, Cheng JX, Kassab GS. 2011 The layered structure of coronary adventitia under mechanical load. *Biophys. J.* **101**, 2555–2562. (doi:10.1016/j.bpj.2011.10.043)
68. Lu X, Pandit A, Kassab GS. 2004 Biaxial incremental homeostatic elastic moduli of coronary artery: two-layer model. *Am. J. Physiol. -Heart Circul. Physiol.* **287**, H1663–H1669. (doi:10.1152/ajpheart.00226.2004)
69. Chen H, Slipchenko MN, Liu Y, Zhao XF, Cheng JX, Lanir Y, Kassab GS. 2013 Biaxial deformation of collagen and elastin fibers in coronary adventitia. *J. Appl. Physiol.* **115**, 1683–1693. (doi:10.1152/japplphysiol.00601.2013)
70. Beamish JA, He P, Kottke-Marchant K, Marchant RE. 2010 Molecular regulation of contractile smooth muscle cell phenotype: implications for vascular tissue engineering. *Tissue Eng. Part B-Rev.* **16**, 467–491. (doi:10.1089/ten.teb.2009.0630)
71. Rensen SSM, Doevendans P, van Eys G. 2007 Regulation and characteristics of vascular smooth muscle cell phenotypic diversity. *Netherlands Heart J.* **15**, 100–108. (doi:10.1007/BF03085963)
72. Rubod C, Boukerrou M, Brieu M, Dubois P, Cosson M. 2007 Biomechanical properties of vaginal tissue. Part 1: new experimental protocol. *J. Urol.* **178**, 320–325. (doi:10.1016/j.juro.2007.03.040)
73. Feola A, Abramowitch S, Jones K, Stein S, Moalli P. 2010 Parity negatively impacts vaginal mechanical properties and collagen structure in rhesus macaques. *Am. J. Obstet. Gynecol.* **203**, 8. (doi:10.1016/j.ajog.2010.06.035)
74. Pena E *et al.* 2011 Mechanical characterization of the softening behavior of human vaginal tissue. *J. Mech. Behav. Biomed. Mater.* **4**, 275–283. (doi:10.1016/j.jmbbm.2010.10.006)
75. Martins P, Silva AL, da Fonseca A, Santos A, Santos L, Mascarenhas T, Jorge RM, Ferreira AJ. 2013 Biomechanical properties of vaginal tissue in women with pelvic organ prolapse. *Gynecol. Obstet. Invest.* **75**, 85–92. (doi:10.1159/000343230)
76. Ulrich D, Edwards SL, Letouzey V, Su K, White JF, Rosamilia A, Gargett CE, Werkmeister JA. 2014 Regional variation in tissue composition and biomechanical properties of postmenopausal ovine and human vagina. *PLoS ONE* **9**, e104972. (doi:10.1371/journal.pone.0104972)
77. Gong RQ, Xia ZJ. 2019 Collagen changes in pelvic support tissues in women with pelvic organ prolapse. *Eur. J. Obstet. Gynecol. Reprod. Biol.* **234**, 185–189. (doi:10.1016/j.ejogrb.2019.01.012)
78. Karam JA, Vazquez DV, Lin VK, Zimmern PE. 2007 Elastin expression and elastic fibre width in the anterior vaginal wall of postmenopausal women with and without prolapse. *BJU Int.* **100**, 346–350. (doi:10.1111/j.1464-410X.2007.06998.x)